5. Study on galling behaviour of HiPIMS deposited Mo/DLC multilayer coatings at room and elevated temperature.

**Work published in Wear [250]*

Galling has been a severe concern in oil – gas, automotive, and nuclear sectors. SS 304 steel is used in these industries despite its low galling resistance because it possesses good corrosion resistance properties. The threads of bolt, nut or a tapped hole and fasteners made of SS 304 experience severe damage due to galling or cold working. Therefore, the galling characteristics of the coated SS 304 samples were studied against the uncoated counterpart. A multilayer coating of molybdenum (Mo) and diamond like carbon (DLC) was deposited through dual sputtering using a high power impulse magnetron sputtering (HiPIMS) power source for graphite target and pulsed DC power source for Mo target. The Mo/DLC multilayer coating was optimized for antiwear and low friction properties. The evaluation of friction properties was done through a nanotribometer. The galling samples of SS 304 steel were prepared following the ASTM G196 standard, and the optimized coating was deposited on the galling samples. The adhesion strength of the coating was analyzed with the help of a nanoscratch tester. The galling behavior of coated and uncoated samples was investigated at room temperature (RT) and 300 °C. Galling damage was quantified by calculating the galling area on the galled sample. Image processing and computer vision tools were used to calculate the galled area. The tribopair having coated (Mo/DLC multilayer coating on SS 304) and the uncoated sample (SS 304) showed lower galled area than the tribopair containing both uncoated samples in every test conditions. At RT the coated sample failed at 15 MPa, whereas the uncoated samples failed at 5 MPa. Similar type of results were obtained when the samples were tested at 300 °C. The characterisation of the coating and the mechanism of galling were

studied in detail with the help of Raman spectroscopy, X-ray photoelectron spectroscopy (XPS), nanoindentation, stereo-zoom optical microscopy, and scanning electron microscopy (SEM).

5.1. Introduction.

DLC coatings are highly explored because of their low friction, high wear resistance, and good hardness. These carbon-based coatings can exhibit a vast range of structures and compositions, resulting in different mechanical and tribological properties. The properties of these carbon-based coatings range from soft graphite-like carbon to hard metal-doped amorphous carbon coatings, also termed as nanocomposite coatings. Different types of multilayer and nanocomposite coatings doped with transition metals (Cr, Ti, W, Ta, Mo, etc.) have been explored for their excellent mechanical and tribological properties [22,73,77,222,251–255]. The properties of DLC coatings are influenced by the sp^3/sp^2 hybridized carbon ratio in the coating [256].

The nanocomposite metal carbide coatings can easily be prepared by sputtering a metal target in the presence of acetylene or methane gas. They can also be prepared by sputtering targets of metal (or metal carbide) and graphite simultaneously or by sputtering a composite target of metal carbide in the presence of acetylene or methane gas to compensate for the lack of carbon from the metal carbide target. The coatings obtained through sputtering a metal (or metal carbide) target and a graphite target is termed as dual sputtering. The other two sputtering processes in the presence of acetylene and methane gases are termed as reactive sputtering. Contrary to dual sputtering, the coatings obtained in reactive sputtering are hydrogenated coatings with hydrogen coming from hydrocarbon gas [257,258]. The presence of hydrogen plays a pivotal role in reducing friction in DLC types of coatings in vacuum conditions. Hydrogen passivates the dangling σ-bonds on the DLC surface and helps in reducing friction

in the vacuum environment [259–261]. Hydrogen-free DLC coatings reduce friction and wear in the ambient environment. Lowering the hydrogen content helps in better wettability of the surface, which increases the adsorption of lubricant on the surface [262].

Hydrogenated DLC is thermally less stable than hydrogen free DLC, as the hydrogen effusion easily occurs from the amorphous matrix at a temperature of 200 °C [179]. Magnetron sputtering is the most common method to deposit such films. It is easy to control the chemical composition and functional properties, and it is easy to scale up industrially. High power impulse magnetron sputtering (HiPIMS) is a variation of magnetron sputtering in which high peak cathode power is applied to the target in very short pulses of duty cycle < 1%. To enhance the tribological properties of DLC films, the sp^3 carbon content needs to be higher in the film. HiPIMS produces a high degree of ionized carbon ions from sputtered neutral carbon, which enhances the sp^3 content in the films [263]. The deposition rate of DLC has always been an issue for researchers as DLC films are brittle and contain high residual stresses [264]. Moreover, the HiPIMS system itself has a low deposition rate. Many investigations in the past have reported dense DLC films deposited through the HiPIMS technique. Still, after an hour of the deposition, the thickness of the film has been considerably less, ranging from 60-300 nm [265,266]. Therefore, various techniques have been used to increase the deposition rate of DLC films, such as co-doping DLC films with transition metals [267,268] and clubbing the HiPIMS deposition system with deep oscillation magnetron sputtering and direct current magnetron sputtering (DCMS) [264].

Galling is a limiting factor for many tribosystems where dry sliding occurs, such as in automotive, oil-gas, medical devices, food processing, sheet metal stamping, and nuclear-powered industries. Commonly, galling occurs when there are high contact pressure and low sliding speed in dry sliding conditions. Galling occurs because of material transfer or plastic deformation, or both. The size of surface protrusions appearing on the galled surface is far

worse than any other form of wear. These surface protrusions take up the running clearance in a tribosystem and lead to the seizure. Some tribopairs (especially stainless steel) tend to form strong adhesive bonds during sliding. A significant amount of material gets adhered to the other surface, creating protrusions on one or both the surfaces of the tribopairs. These surface protrusions are the primary criteria for deciding if galling has occurred or not. Galling damage can be mitigated by formation of oxide layers on the surface, use of flouro-based polymers, and coating the surface with hard carbides or nitrides [269–271]. In the past, Heinrichs et al. [272,273] and Podgornik et al. [274–276] tried to improve the galling resistance of forming tool in the cold forming of aluminum and steel, respectively, by coating the forming tool with different types of industrial based coatings (TiN. DLC, TiAlN, TiCN, etc.), and by altering the roughness of the forming tool. A load scanning test rig comprising two crossed cylinders in sliding contact was used to verify the galling tendency of the coated forming tool by varying the contact pressure between 1-3.5 GPa. The galling properties were qualitatively compared for various coatings by comparing the material transfer during the tribotesting. The identification of the galling is subjective, and over the years, the definition of the galling has been modified. According to ASTM G40-15 standard, the definition of galling is as follows [277]:

Galling, n - a form of surface damage arising between sliding solids, distinguished by macroscopic, usually localized, roughening, and the creation of protrusions above the original surface; it is characterized by plastic flow and may involve material transfer.

ASTM G98 and ASTM G196 are the standards generally used for galling tests [6,7]. Budinski et al. [278], while testing according to ASTM G98 and G196 standards reported that the galling damage can be interpreted by scoring the different types of surface damages (burnishing, scoring, wear, incipient galling, and adhesive transfer) occurring in the tribosystem. Hummel et al. [279] identified the problems persisting with the ASTM G98 standard and proposed the

ASTM G196 standard for calculating the threshold galling stress. Also, the new ASTM G196 standard ensured that the test geometry has a uniform stress distribution and does not contain a region of zero sliding distance (also known as dead zone present at the center), which was present in ASTM G98 standard.

The present investigation focused on developing and optimizing multilayer Mo/DLC thin film coating to improve wear resistance through HiPIMS and examine the galling resistance of the optimized coating at RT and 300 °C.This required many experiments to investigate the effect of parameters like frequency, duty cycle, power level, deposition time, operating pressure, etc., to achieve a highly adherent coating using HiPIMS. As discussed earlier, the HiPIMS process generates dense films, but the deposition rates are relatively low. Therefore, Mo layers of comparable thicknesses were introduced between the DLC layers to generate a thick coating for industrial applications. Adding soft Mo layers between hard DLC layers also reduces the internal stresses in the coating, which helps in creating thick coatings having good adhesion to the substrate [229,234,280]. Also, Mo forms an oxide MoO_3 at 300 °C, which is lubricious and leads to good tribological properties at high temperatures [133,138]. In the present investigation, the authors have attempted to combine the benefits of coating deposited through HiPIMS and soft Mo layers to develop a novel multilayer Mo/DLC thin film coating capable of operating at room and high temperatures. The mechanized galling test rig developed by Harsha et al. [8] can identify the occurrence of galling through a rise in frictional torque measurements to assess the galling performance of multilayer Mo/DLC coating on SS 304 samples. ASTM G196 standard requires a large number of samples for reporting the galling resistance of material pairs. Therefore, coating many samples with a laboratory based sputtering system was not possible. However, test specimens were prepared according to ASTM G196. The frictional torque measurements ascertained the galling occurrence of Mo/DLC coating. The experimental data generated for different grades of stainless by Harsha

et al. [8,281] (as per ASTM G196 standard) were used as reference. Daure et al. [282] used the variation in frictional torque data to investigate the galling behavior of Stellite 6 (Co-based) and Tristelle 5183 (Fe-based) materials. However, the tests conducted by Daure et al. were only for one rotation, and the variation of frictional torque was not enough to identify the occurrence of galling during testing. Rogers et al. [283] quantified the galling damage in SS 316 by quantifying the area of the galled surface. In the present investigation, the combination of frictional torque measurements and galled surface area was used to assess the performance of Mo/DLC multilayer coating with uncoated SS 304 steel at room temperature (RT) and 300 °C. The samples were given multiple rotations till they failed due to galling. Since the tests were also conducted at 300 °C, the multiple cycles helped to overcome the oxide layer effect [281,284].

5.2. Experimental details.

Silicon (Si) wafers were used to optimize Mo/DLC multilayer coating to achieve a low coefficient of friction and wear among the coated samples. A balanced magnetron sputtering system equipped with two targets (of size 3 inches) was used for the deposition of Mo/DLC film. The Mo target was powered by a pulsed DC power source, whereas the HiPIMS power source (Ionautics, SOLVIX) was used for the graphite target. The HiPIMS power source operated at the maximum power of 5 kW with peak current and voltage output of 600 A and 1000 V, respectively. Before deposition, ultrasonic cleaning was done for silicon substrates with isopropyl alcohol and acetone for 30 minutes. Substrates were loaded in the vacuum chamber (with a substrate to target distance of 8 cm), and the chamber was evacuated to the base pressure of 5.0×10^{-6} mbar. The substrates were sputter etched for 30 minutes in an argon plasma at a DC bias voltage of -850 V. To improve the adhesion of the coating, an interlayer of Mo was deposited on the substrates. The Mo interlayer was deposited for 5 mins at a power

of 100 W. Then DLC and Mo layers were deposited alternately. Table 1 shows the detailed deposition parameters. The DLC films were optimized by varying the argon flow rate into the vacuum chamber.

A nanoindentation tester (CSEM) was used for hardness measurements. The instrument uses a Berkovich diamond indenter, having a resolution of 0.04 nm and a force resolution of 0.04 μN. The maximum load applied by the indenter was 3 mN in all 8 indentations to ensure that the indenter should not penetrate more than $1/10^{th}$ of the thickness of the coating. The loading and unloading curves obtained from the instrument were then used to calculate the hardness and elastic modulus of the coating using the Oliver Pharr method [214].

The thickness and cross-sectional morphology of the coating were studied using the field-emission scanning microscopy (FESEM). Raman spectroscopic studies of the as-deposited coating were done by a commercial micro-Raman spectrometer equipped with a laser of 532 nm wavelength (LabRam, HR Evolution). SPECS X-ray photoelectron spectroscopy (XPS) was used to obtain the XPS spectrum of the Mo/DLC film to calculate the sp^3carbon percentage in the film. The instrument uses an Al K_α non-monochromatic radiation as a source, operating at 150 W (12 kV, 12 mA). The binding energy of the peaks obtained in this investigation was referenced with the C1s peak at 284.6 eV.

The friction and wear tests were carried out on a CETR-UMT nanotribometer. Since the coatings obtained under different flow rates had considerably higher hardness than stainless steel, balls having comparable hardness to the coating were chosen to evaluate the friction and wear characteristics. Mo/DLC coated silicon wafers were tested against a tungsten carbide ball (hardness ~ 15 GPa) of 4 mm diameter under reciprocating sliding conditions. The normal load applied was 2 N, corresponding to maximum Hertzian contact stress of 1.3 GPa. A sliding speed of 6 mm/sec and a stroke length of 3 mm corresponding to the frequency of 1 Hz, applied

to the reciprocating arm, were used for the tests. All the friction and wear tests were carried out at room temperature for 30 mins. The two-dimensional profiles of the wear scars were mapped by a profilometer (Nano Map 500 LS, AEP Technology).

The galling samples were prepared as per the ASTM G-196 standard. The samples were machined from the hexagonal bar of SS 304 and had a roughness of 0.5 µm. SS 304 samples of size 25 X25 X 5 mm^3 were prepared for scratch testing and had a similar roughness as the galling samples. The SS 304 samples had hardness and elastic modulus around 1.3 and 210 GPa, respectively. The chemical composition of SS 304 samples mainly comprises of iron (69 wt%), nickel (10 wt%), chromium (18 wt%) and carbon (0.07 wt%). The samples for galling and scratch testing were coated similarly to silicon substrates, and the number of stacks of Mo/DLC layers was increased. The deposition time was twice what was used for coating silicon substrates. The roughness of the galling samples was 60 nm after the deposition of the coating.

Table 5.1. Deposition parameters for Mo/DLC coatings for a single layer.

Parameters	Molybdenum Target	Graphite Target
Power (W)	100	150
Voltage (V)	224.3	862
Current (A)	0.36	7.00
Frequency (Hz)	100000	250
Pulse duration (seconds)	0.00300	0.00005
Argon flow rate (sccm)	12.5	8,10,12.5,15,18
Deposition Time (minutes)	3	20

Scratch tests were carried out on a CETR-UMT nanoscratch tester equipped with a spherical diamond tip indenter with a tip radius of 5 µm. The load was varied from 0-2 N at a loading

rate of 3 N/min and a scratch speed of 0.1 mm/sec. The critical scratch loads (Lc_1) and (Lc_2) were calculated with the help of acoustic emission data from scratch. The internal stress of the film was calculated with the help of Stoney's equation [285] by measuring the bending of the coated silicon substrate with the profilometer. Stoney's equation is given as:

$$\sigma = \frac{E_S}{6(1-\vartheta_S)}\left(\frac{t_S^2}{t_f}\right)\left(\frac{1}{R_2}-\frac{1}{R_1}\right)$$

where σ is the internal stress, E_s and υ_s being the modulus of elasticity and Poisson's ratio of the substrate material, R_1 and R_2 are curvatures of the substrate before and after deposition, and t_s and t_f are the thickness of substrate and film, respectively.

Galling tests were conducted in a galling test rig (DUCOM Instruments) according to ASTM G196. **Figure** 5.1 shows the setup of the galling tester with heater. The samples were aligned with the help of an alignment pin, as shown in **Figure** 5.1(b), the top sample was stationary and the lower sample was rotated. A detailed description of the experimental setup can be found in the section 3.6.4. Three types of tribopairs were tested 1) steel against steel samples, 2) steel against Mo/DLC multilayer coated samples, and 3) Mo/DLC multilayer coated sample against itself. However, tests for Mo/DLC multilayer coated sample against itself were not reported because they suffered heavy damage at low stresses (lower than steel against steel samples). The samples underwent severe adhesive wear because of strong adhesive contact between similar surfaces and low roughness values, making it difficult to compare the galling performance of coated substrates. Tests were conducted at RT and 300 °C, with a rotation speed of 6 rpm corresponding to the average sliding velocity of 3 mm/sec. The load was increased from 2 to 15 N (corresponding contact pressure of 2 to 15 MPa) until the tribopair started failing within one rotation or 10 seconds. The tests at each load were conducted till large fluctuations in friction torque were observed. Each test was repeated four times to confirm the accuracy of

the results obtained. The comparison between the two tribopairs was made based on the highest load needed for the tribopair to fail within one rotation and the area of the galled surface obtained after the failure of the tribopair. ImageJ software was used to approximate the galled surface area. The stereo-microscopic images of the galled surface were converted to 64 bit black and white images so that features of the worn surfaces do not get lost. The brightness, contrast, sharpness, and threshold of the images were adjusted to cover the worn surface area in white and keep the other part of the image entirely black. A python-based computer vision program was used to calculate the number of white pixels, then converted into the area.

The silicon substrates were used instead of SS304 substrates to optimize the coating, so adhesion of coating can be a concern during various tribotestings. Silicon substrates make it easier to determine the thickness of the coating during the optimization on silicon substrates either by masking the substrate or fracturing it to study the cross-section through electron microscopy. It was believed that the properties of Mo/DLC multilayer coating on SS 304 and silicon substrate were the same because the standard operating procedure was used for the deposition of the optimized coating on SS 304 substrates for galling experiments. Also, almost a similar substrate size as galling sample was used for the optimization experiments (~100 mm^2) to avoid the effect of stress on adhesion. The roughness of the SS 304 substrate was much higher (0.5 µm) than the silicon substrate (3 nm). This enhanced roughness of SS 304 helps in improving the adhesion of Mo/DLC multilayer coating through mechanical interlocking at the interface between the substrate and the coating. Also, adhesion affects the tribological properties when the coating starts delaminating during the tribotesting. However, none of the coatings showed signs of delamination during tribotesting.

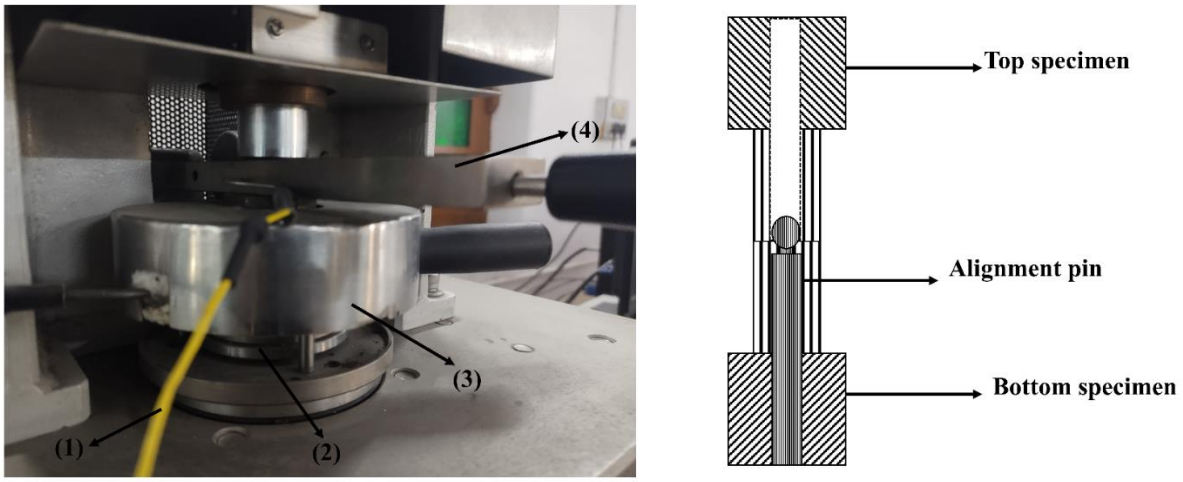

Figure 5.1. (a) Setup of galling tester 1) Thermocouple, 2) rotating table, 3) specimen heater, 4) top specimen holder for frictional torque measurement; 1(b) cross-sectional view of aligned samples inside the heater.

5.3. Results and discussion.

5.3.1 Microstructure of the coating.

5.3.1.1. Cross-section of the coating.

Figure 5.2 shows a typical cross-section FESEM image of the Mo/DLC coating. The coating has a thick Mo interlayer for better adhesion, followed by DLC (3 layers)/Mo (2 layers) multilayer arrangement. The thickness of the coating varied from 800 to 1200 nm because of the variation in deposition rate of DLC layers at various argon flow rates. The Mo layer deposited through pulsed DCMS clearly shows significantly high deposition rates than the DLC layer deposited through HiPIMS. The deposition rate of DLC increased from 7 to 13 nm/min, with an increase in argon gas flow rate from 8 to 18 sccm. The Mo layer showed columnar growth in all the coatings, whereas the DLC layer showed a highly dense structure.

The highly dense structure of DLC is due to the high ionization ability and low deposition rates of the HiPIMS system. For galling and scratch testing of the Mo/DLC coating, 6 DLC layers of around 216 nm each and 5 Mo layers (excluding Mo interlayer) of ~100 nm each were deposited at the optimized argon gas flow rate of 15 sccm (**Figure** 5.3). The total thickness of the coating for samples of galling and scratch tests was around 2 µm.

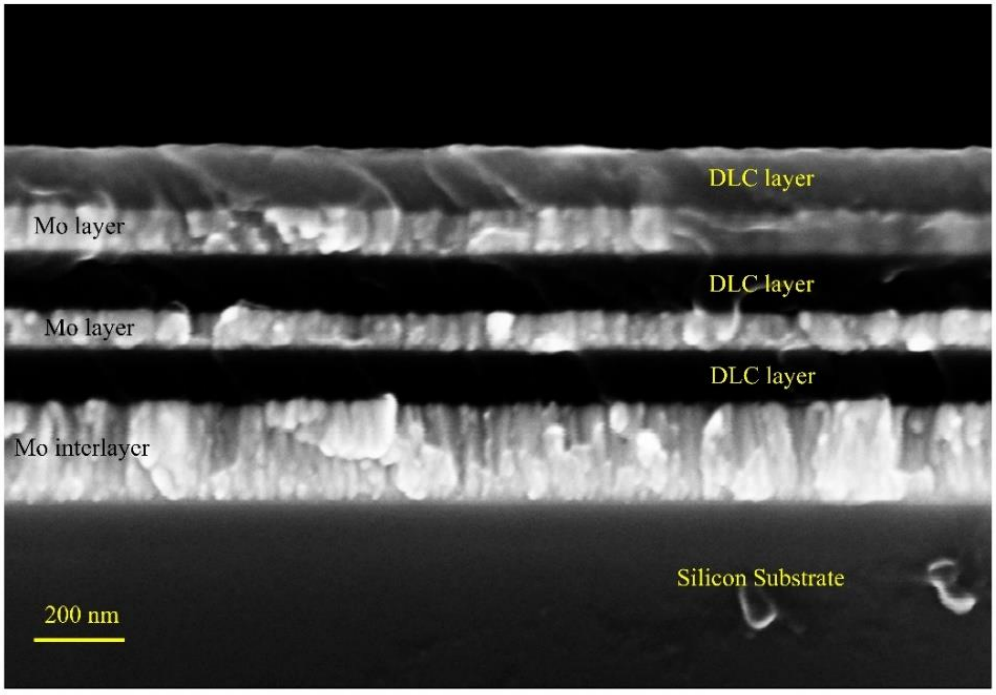

Figure 5.2. FESEM of cross-section of the Mo/DLC coating.

5.3.1.2. Raman and x-ray photoelectron spectroscopy studies of the Mo/DLC multilayer coating.

Raman spectroscopy is a non-destructive and very efficient tool to study the structure of carbon materials. The occurrence of the D band (1360 cm^{-1}) and G band (1580 cm^{-1}) is the common characteristic of the Raman spectrum of DLC coatings. The occurrence of the D peak is due to the defects in the sp^2 hybridized carbon, which is attributed to disordering and less clustering of carbon atoms. The G peak occurs because of the bond stretching of sp^2 hybridized carbon atoms in rings and chains, which comes from the graphite structure [263]. Therefore, many

researchers have often related the D and G peaks to those originating from sp^2 and sp^3 hybridized carbon atoms, respectively. **Figure** 5.4 shows the shift of D and G peaks in the Raman spectrum of Mo/DLC multilayer coating deposited at different argon flow rates.

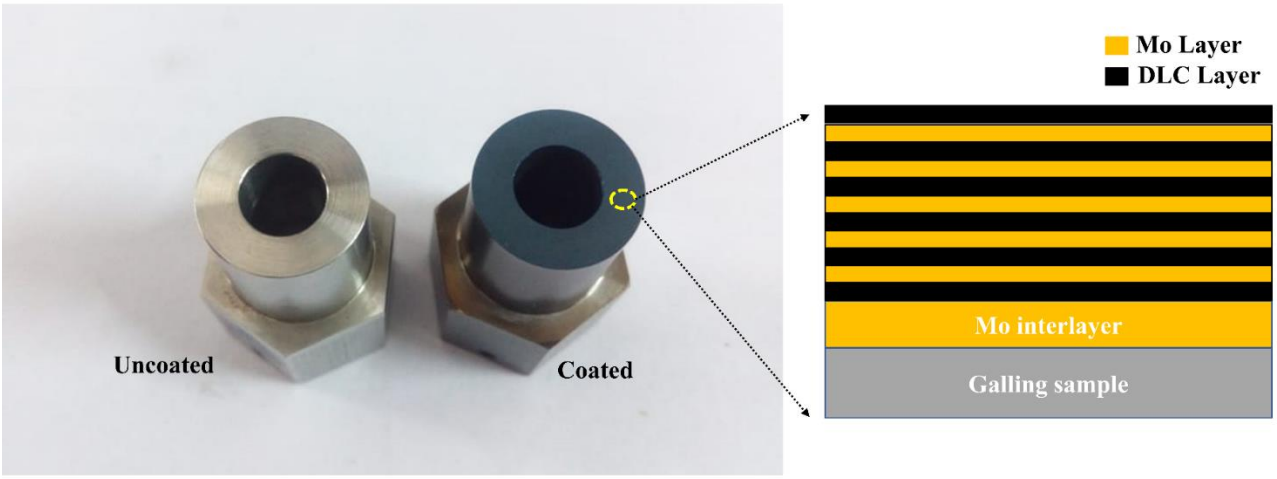

Figure 5.3. (a) Image of the coated and uncoated samples, (b) schematic representation of layers of coating on a galling sample.

The ratio of sp^3/sp^2 hybridized carbon in the amorphous carbon matrix can be qualitatively associated with the intensity ratio of the D and G peaks (I_D/I_G) and the shifting of the G peak position. The films containing more percentage of sp^3 carbon have a lower I_D/I_G ratio, and the G peak also shifts to lower wavenumber. The Raman curves were fitted by a Gaussian function and deconvoluted into the respective peaks to calculate the I_D/I_G ratio and the shift in the G peak position. A typical deconvoluted spectrum is shown in **Figure** 5.5. Apart from the characteristic D and G peaks, two more peaks were observed on deconvoluting the Raman spectrum of different coatings. The positions of the deconvoluted peaks were observed in the wavelength ranges of 1160-1190 cm^{-1} and 1490-1530 cm^{-1} in different spectra. The peak centered at 1160-1190 cm^{-1} is due to transpolyacetylene chains; this peak shifts to lower wavelengths when the laser of lower wavelength is used [265]. This structure contains sp^2 and

sp^3 hybridized carbon atoms connected through chains of different lengths and compositions [286].

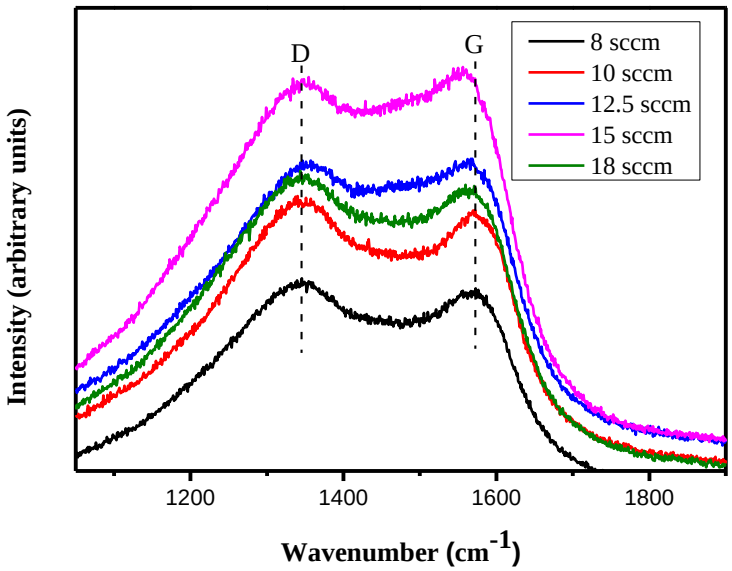

Figure 5.4. Raman shift of D and G peaks for coatings prepared at different argon flow rates.

Similarly, the peak centered at 1490-1530 cm^{-1} occurs due to the amorphous carbon existing in the form of interstitial defects outside the planes of aromatic rings linked by sp^3 hybridized carbon atoms [286]. **Figure** 5.6 depicts the I_D/I_G ratio trend and G peak position for different argon flow rates. The film deposited that 15 sccm flow of argon gas exhibited least I_D/I_G ratio and the highest redshift in G peak position, which means qualitatively the film deposited at the argon flow rate of 15 sccm had the highest sp^3 carbon percentage with respect to the other films deposited at different flow rates. XPS analysis was carried out on the films deposited at 12.5, 15, and 18 sccm flow rates of argon gas, to quantify the percentage of sp^3 hybridized carbon in the Mo/DLC multilayer coatings.

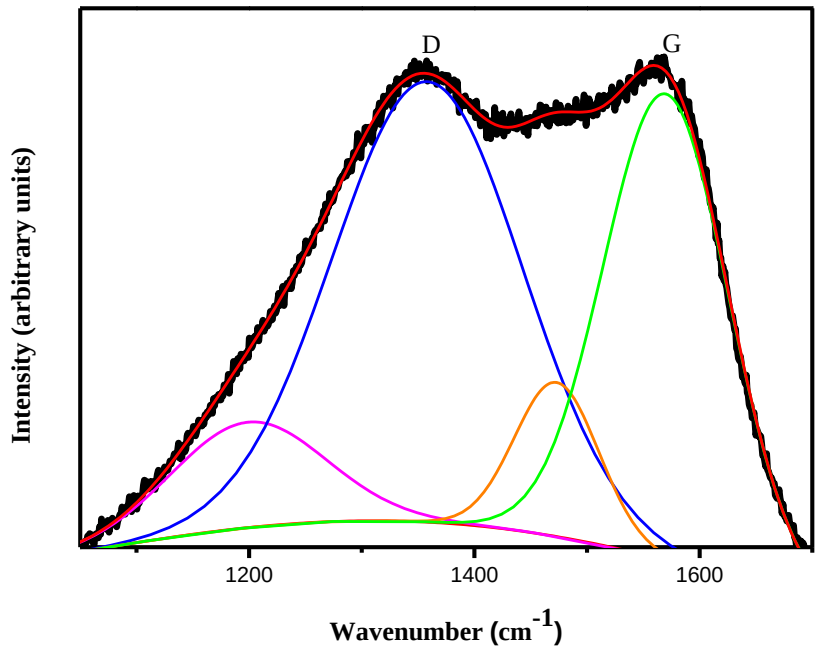

Figure 5.5. Deconvoluted spectrum of Mo/DLC multilayer coating deposited at 8 sccm of argon flow rate.

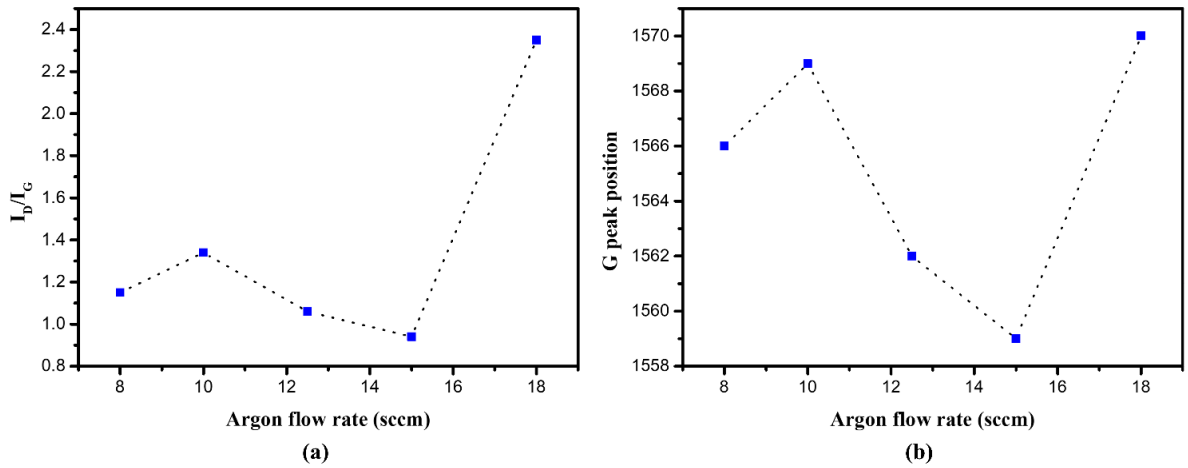

Figure 5.6. Variations of (a) I_D/I_G ratio and (b) G peak position with respect to argon flow rate.

XPS analysis was carried out to know the percentage of sp^2 and sp^3 hybridized carbon in the DLC coating. The C1s spectrum of Mo/DLC coating is shown in **Figure** 5.7. After fitting the

spectrum with the Gaussian function, three major deconvoluted peaks were observed. The peaks were centered at approximately 284.5, 285.9, and 288.0 eV, corresponding to the sp^2 C-C, sp^3 C-C, and C-O bond, respectively. The small peak corresponding to the C-O bond exists because of the surface adsorption of oxygen on the coating surface. However, no peaks corresponding to Mo were found in the XPS analysis of Mo/DLC coating. In XPS, only a thin top layer of the coating is analyzed. Since the top layer consisted of the DLC layer, the presence of the Mo layer would have been masked by it. The sp^3 carbon percentage in the coating was calculated from the ratio of areas of the curves, i.e., area of sp^3 curve / (total area of the curve). The highest sp^3 percentage of 64 percent was obtained for coating deposited at an argon flow rate of 15 sccm, which was relatively higher than the sp^3 percentage reported by other investigators through the HiPIMS process [177,268,287]. The coatings deposited at 12.5 and 18 sccm flow rates had 45 and 31% of sp^3 carbon, respectively. The sp^3 carbon percentage trend followed the trend in the I_D/I_G ratio curves and the shift in the G peak's position of the Raman spectrum. The I_D/I_G ratio started decreasing below the flow rates of 10 sccm too. However, the reason for not considering the characterization of the coatings at lower flow rates is the coating stability during the wear testing, which will be discussed in the subsequent sections.

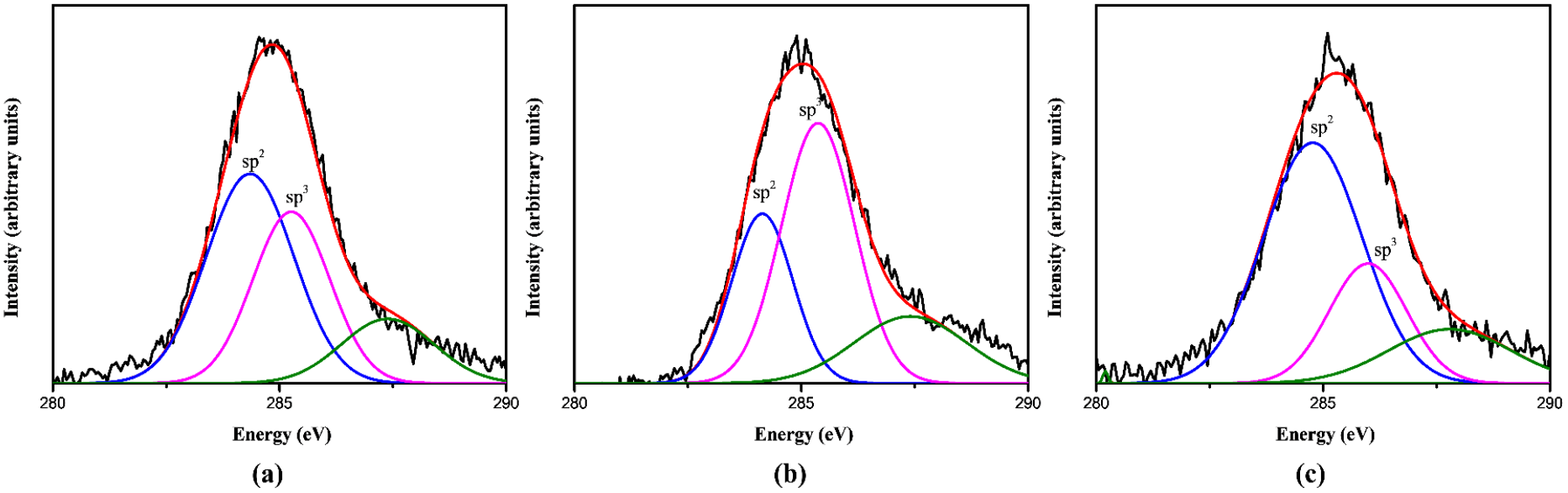

Figure 5.7. XPS C1s spectra of coating deposited at argon gas flow rates of (a) 12.5 sccm (b) 15 sccm and (c) 18 sccm.

5.3.2 Mechanical and tribological characterization of Mo/DLC multilayer coating.

5.3.2.1. Hardness of the coating.

The effect of the argon flow rate on the hardness of the Mo/DLC multilayer coating is demonstrated by the load-displacement curve in **Figure** 5.8. The coating deposited at a 15 sccm flow rate shows the least displacement, leading to the coating with the highest hardness of 21 GPa. The hardness increased when the flow rate was increased from 10 to 15 sccm but decreased significantly to 8 GPa when the flow rate increased to 18 sccm. An increase in hardness was observed when the coating was deposited at flow rates lower than 10 sccm, which was in agreement with the results obtained by Takumi et al. [177]. However, the coating deposited at low pressure caused heavy arcing in the system, was uneven, and a gradual color change was also observed on the coating surface. Moreover, the coating also peeled off completely when it was left idle for two days after tribotesting. Therefore, the high hardness value can be attributed to the high internal stress in the coating deposited at lower flow rates, which leads to peeling off later.

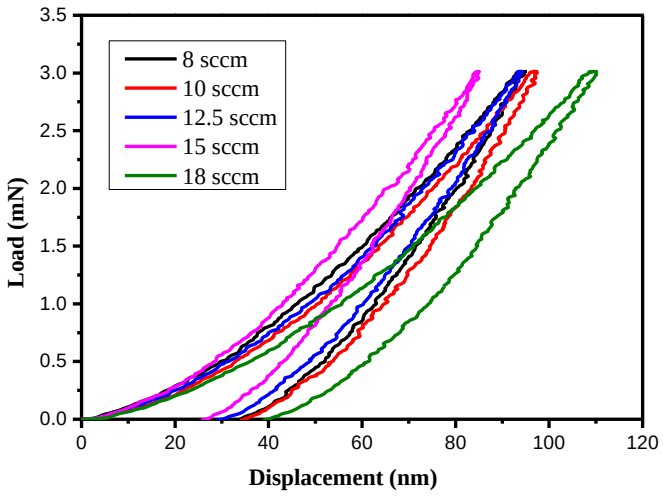

Figure 5.8. Load vs displacement curves of Mo/DLC multilayer coatings at different flow rates.

5.3.2.2. Friction and wear results.

Figure 5.9 shows the variation of CoF in the coatings deposited at various flow rates obtained from nanotribometer. The coating deposited at a flow rate of 8 sccm failed at the initial stages of the wear testing. The CoF seemed to be stabilized for higher flow rates. The CoF of the coating deposited at 10 sccm flow rate seemed to be partially stabilized but with several spikes in CoF during the tribo-testing. The CoF of coatings deposited at 12.5, 15, and 18 sccm of Ar flow rates did not show any peaks. Many investigations have already been reported on the tribological behaviour of the DLC type of coatings [39,174,176,263]. The formation of the DLC transfer layer on the counter surface has been the main reason for low friction and wear. The wear profiles of coatings deposited at different flow rates are shown in **Figure** 5.10. Coating deposited at 10 sccm Ar flow rate showed the highest wear, which can be attributed to the continuous disruption of the transfer layer. This can also be observed from the presence of peaks in the graph of CoF (**Figure** 5.9). It has been reported that the higher values of H/E (resistance to elastic deformation) and H^3/E^2 (resistance to plastic deformation) result in lower wear rates [114]. The material with high H/E and H^3/E^2 values distribute the load over a larger area, and they respond to an external force due to elastic recovery rather than plastic deformation [288]. The coating deposited at 15 sccm flow rate had the highest H/E and H^3/E^2 values (**Figure** 5.11) and showed the lowest CoF and wear. Coating deposited at 18 sccm flow rate exhibited lower H/E and H^3/E^2 values than the coating deposited at 10 sccm flow rate, but the wear observed in the coating deposited at 10 sccm is much more than the one deposited at 18 sccm. Therefore, the antiwear characteristics of the coating not only depend on the H, E, H/E, and H^3/E^2 values, but also on the formation and disruption of the transfer layer in a DLC coating. Hence, the optimum value of friction and wear were observed at the coating deposited at 15 sccm of the argon flow rate. This optimized coating was then studied for galling experiments at RT and 300 °C.

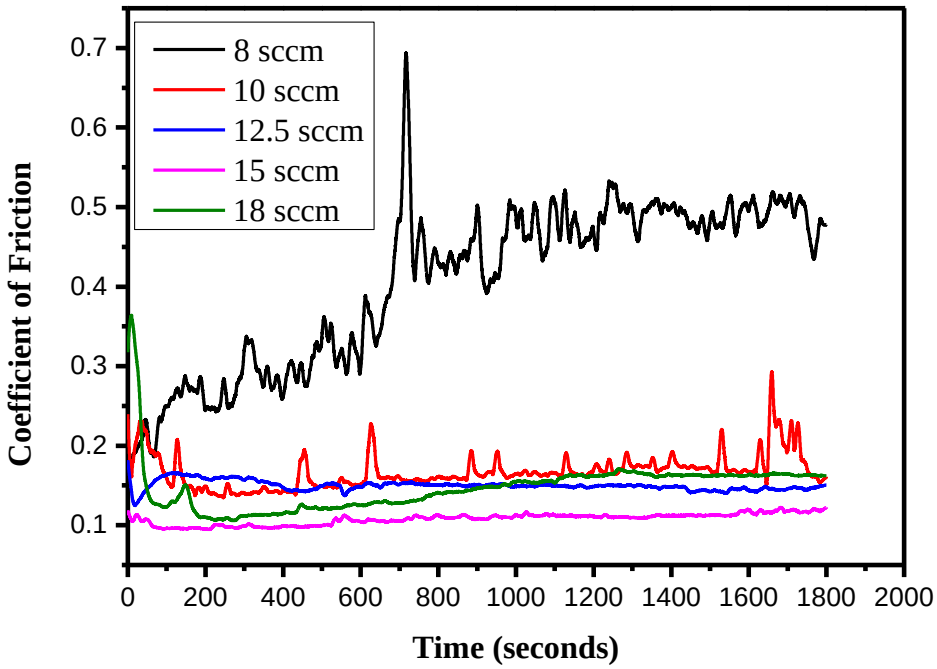

Figure 5.9. Coefficient of friction of Mo/DLC multilayer coating deposited at various argon gas flow rates.

5.3.2.3. Adhesion strength of the optimized coating for galling tests.

The thick coating has a greater tendency of getting delaminated from the substrate. The galling samples contained more layers; therefore, the adhesion strength of the thick coating over SS304 was evaluated. The coating was deposited at an argon flow rate of 15 sccm. The thickness of the coating for the scratch test was same as that on the galling samples. The acoustic emission data shown in **Figure** 5.12 comprises of peaks occurring at different loads, which occurs whenever the coating cracks. Scratch test is generally characterized by the occurrence of critical loads, Lc_1 and Lc_2, where Lc_1 and Lc_2 correspond to the load where the first crack initiates and complete failure of the coating takes place, respectively. From **Figure** 5.12, the first peak, i.e., the initiation of crack occurred at a load of 0.88 N (Lc_1), corresponding to

maximum Hertzian contact stress of 58.8 GPa, while the load at which coating fails is the load at which the acoustic emission data has the highest peak. The highest

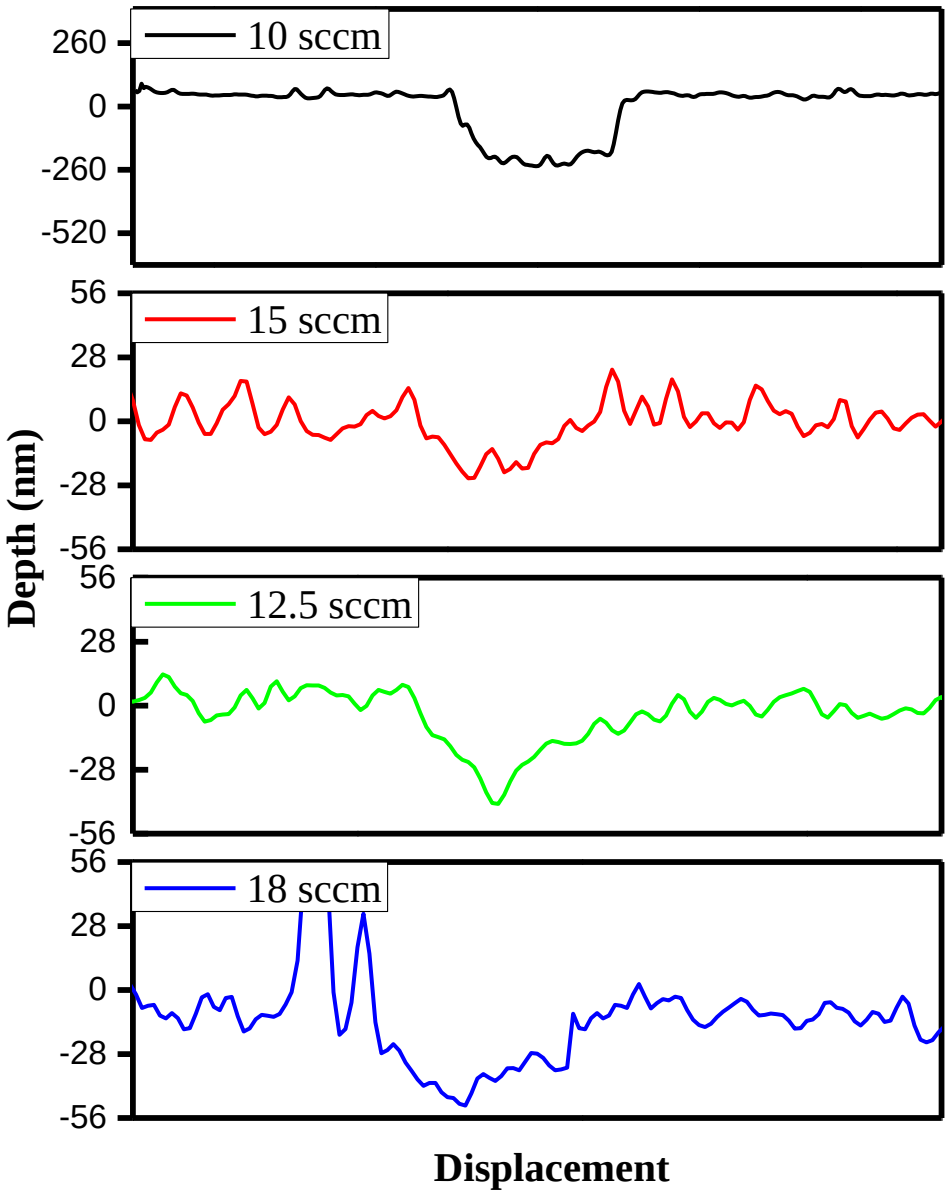

Figure 5.10. Wear depth profiles of coatings deposited at different argon flow rates.

peak was observed at 1.4 N (Lc_2) load, corresponding to the maximum Hertzian contact stress of 68 GPa. The brittle nature of the DLC resulted in constant cracking once the crack was formed. Therefore, many small peaks were observed in the acoustic emission data due to the high sensitivity of the sensor. The scratch test shows that the coating used for galling testing had excellent adhesion on the substrate even after doubling the thickness. The internal stress of the coating used for galling testing was found to be -454 MPa. The internal stress found was on the lower side when compared with the other carbon-based hard coatings [285,289]. The presence of thick metal layers of Mo leads to a lower value of internal stresses in the coating leading to good adhesion to the substrate. Generally, the industrial coatings require a substrate roughness less than 0.2 µm [272,273], but the multilayer Mo/DLC coating showed good adhesion even when the substrate's roughness was around 0.5 µm.

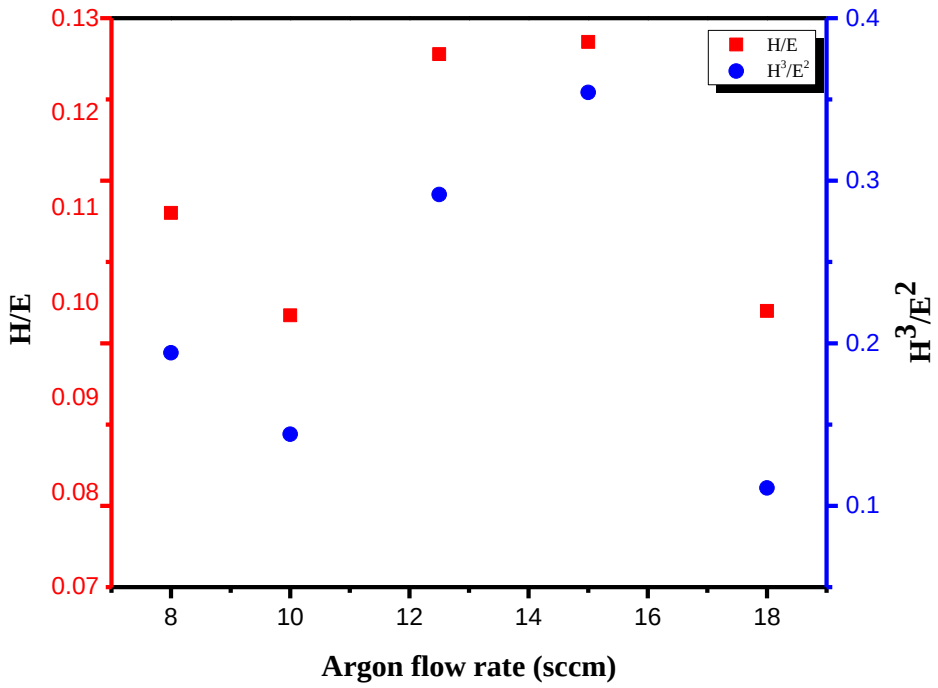

Figure 5.11. H/E and H^3/E^2 values of Mo/DLC coating deposited at different argon flow rates.

5.3.2.4. Galling test at RT.

The occurrence of galling was identified with the rapid and sudden increase in the fluctuations of friction torque with respect to time. The friction torque curves at RT are shown in **Figure** 5.13. The galling is denoted by the letter *G'* in the figures. The steel on steel tribopair failed at the applied stress of 5 MPa in one rotation, and it is in agreement with the observations made by other researchers [8,290]. For the steel on Mo/DLC multilayer coating tribopair, the friction torque data showed heavy fluctuations after 40 seconds for 5 MPa. Galling occurred after 4 rotations for the coated samples. At 10 MPa, the coated samples failed after 2 rotations. The steel on steel tribopair failed with severe surface damage within one rotation (**Figure** 5.14 (d)). The load was increased until the coated substrates started failed within one rotation. At 15 MPa the friction torque of the coated sample against steel tribopair showed a similar observation as steel on steel tribopair at 5 MPa. The coated samples started failing within one rotation at 15 MPa.

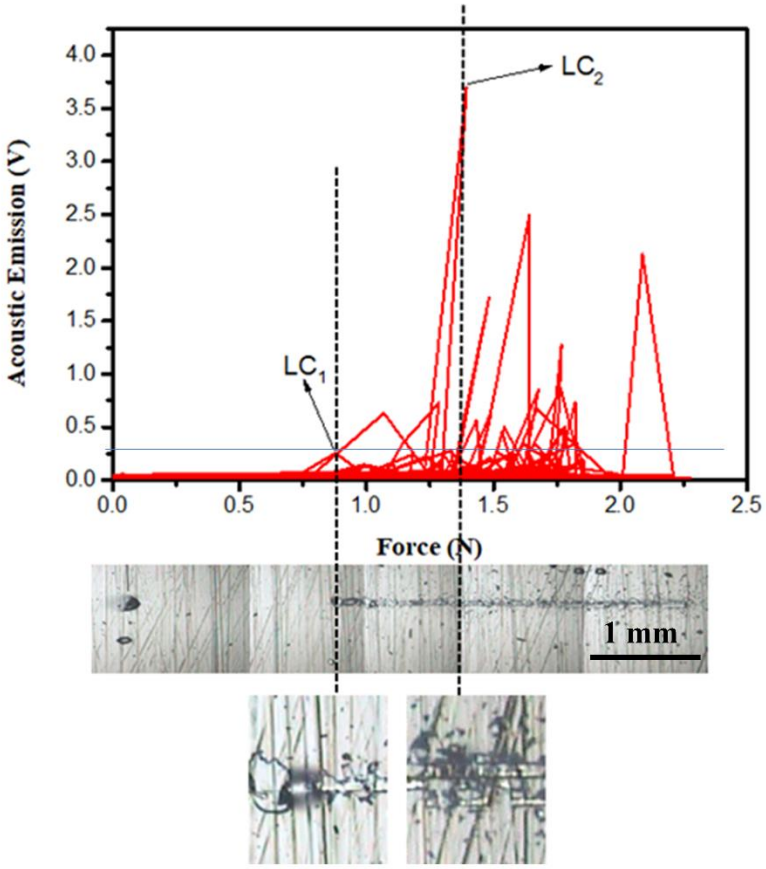

Figure 5.12. Acoustic emission data and optical images of the scratch with magnified images of the scratch at bottom.

The stereo-zoom microscopic images shown in **Figure** 5.14 depict the galled surfaces at different loads and temperature. The galled area on coated substrates appeared to be smaller than the galled area of steel at the same load and temperature, even when the steel on steel tribopair was tested just for one rotation. **Figures** 5.14 (a) and (f) show the coated substrate and its uncoated counterpart tested at 5 MPa, respectively. No signs of galling can be seen from **Figure** 5.14 (a) and (f). However, at higher magnification, material removal was

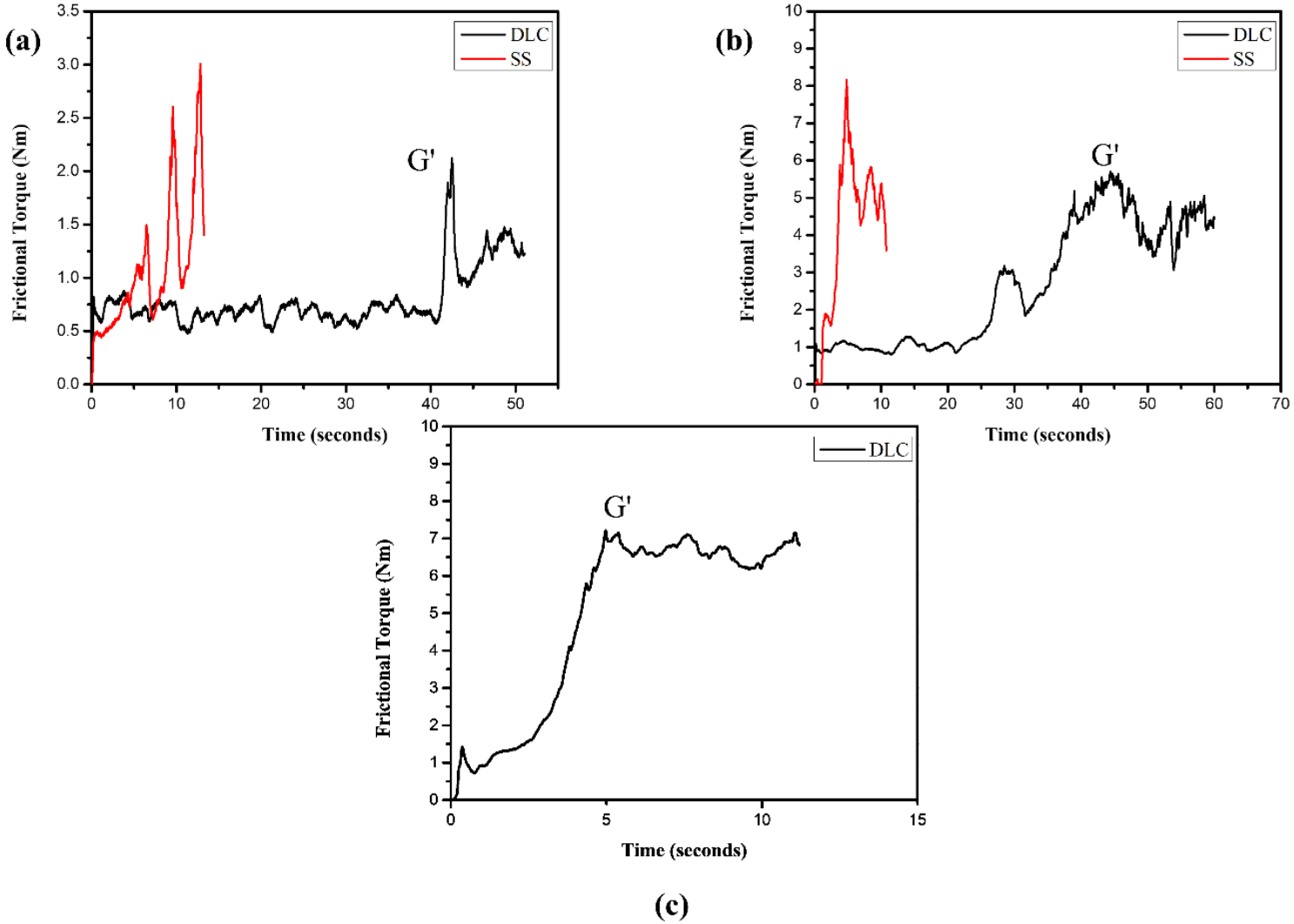

Figure 5.13. Friction torque curves obtained for the two tribopairs at room temperature at (a) 5 MPa (b) 10 MPa and (c) 15 MPa.

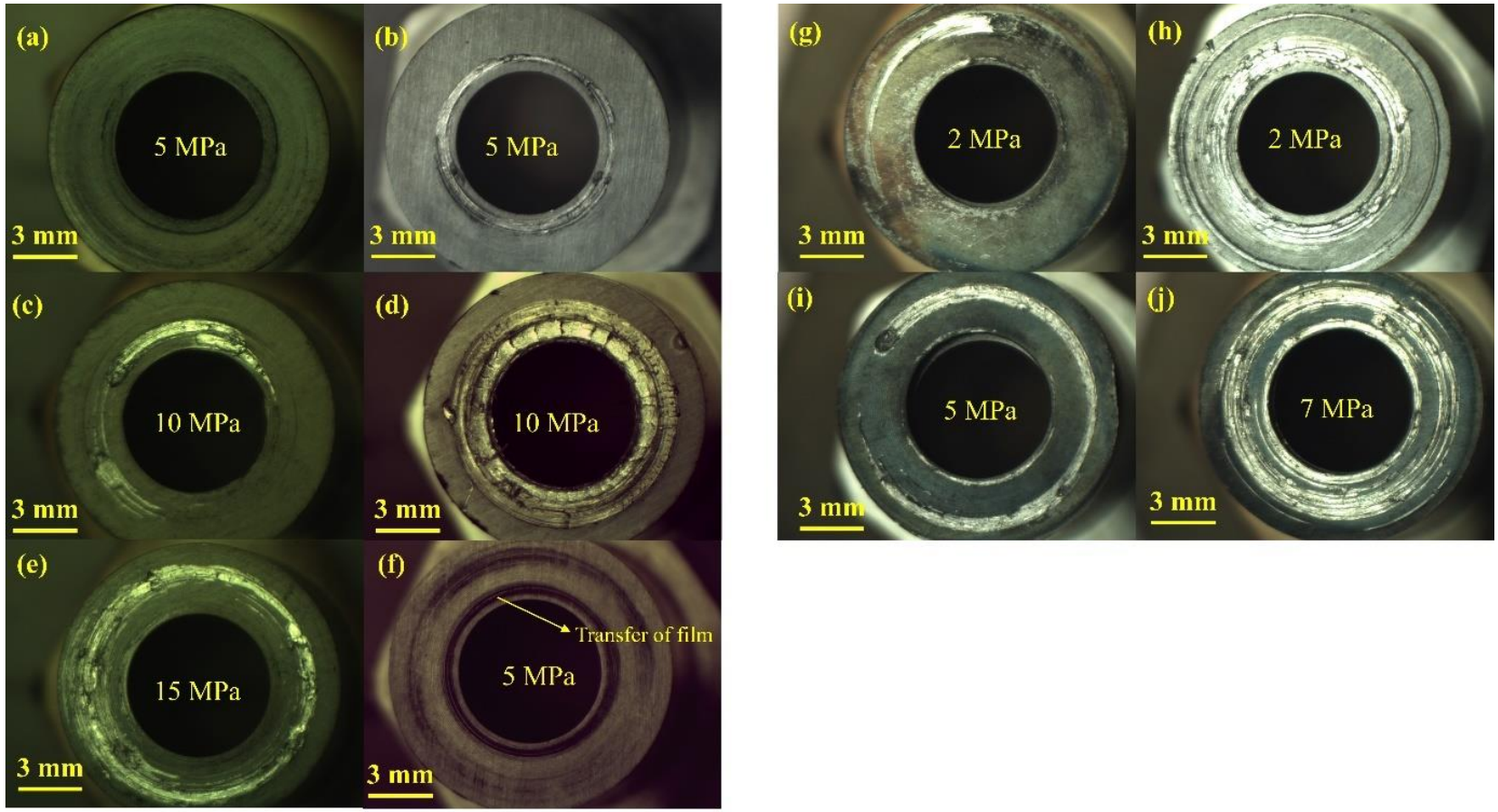

Figure 5.14. Stereozoom microscopic images of the galled samples at RT (a-f) and at 300 °C (g-j).

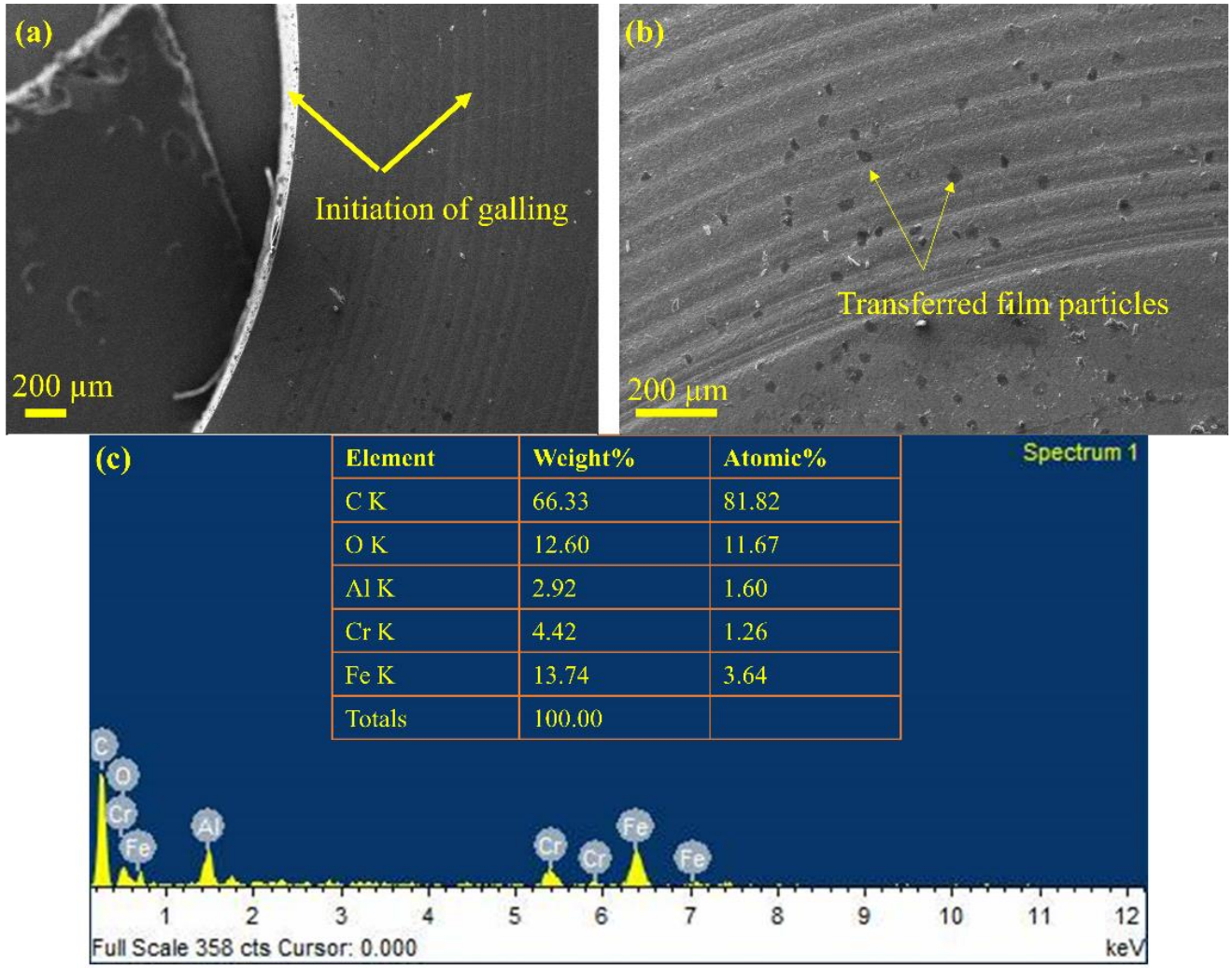

Figure 5.15. (a) FESEM image of the galled sample at 5 MPa load, (b) FESEM image of steel counterpart at 5MPa showing transferred layer, and (c) EDX spectrum of transferred layers.

observed on the surface and near the inner circle of both the specimens (**Figure** 5.15(a)). The tests were stopped. at that instance because there was a significant variation in frictional torque values, preventing further damage at 5 MPa load. This also helped to study the mechanism of the coating during galling tests. The steel counterpart of the steel on Mo/DLC multilayer coating tribopair (**Figure** 5.14 (f)) showed black annular rings after the galling tests. These black annular rings were then analyzed through FESEM and EDAX analysis (**Figure** 5.15(b) and (c)). The black annular rings showed a very high percentage of carbon than the amount present in the steel. This indicates the transfer of the coating layer from the coated substrate to the steel counterpart. The formation of a transfer layer on the counter surface is one of the mechanisms of DLC films to reduce wear and friction, which also helped in improving the galling resistance of steel.

5.3.2.5. Galling test at 300 °C.

When the samples were tested at 300 °C, the galling resistance decreased drastically. The steel on steel tribopair failed within a single rotation at 2 MPa. Whereas, steel on Mo/DLC multilayer coating tribopair failed within one rotation at 7 MPa (**Figure** 5.16). The steel on Mo/DLC multilayer coating tribopair failed after five rotations at 2 MPa (**Figure** 5.16 (a)). There was a drastic change in the galling behaviour of the coating with an increase in applied load. The coating survived for two rotations at 5 MPa but failed within one rotation at 7 MPa. The failure of steel on steel tribopair at the load of 2 MPa is due to the reduction in strength and hardness of the steel at higher temperatures, which results in severe plastic deformations. For steel on Mo/DLC multilayer coating tribopair, high temperature can result in tribochemical reactions at the contact zone. XPS studies were done for the samples galled at high temperatures. **Figure** 5.17(a) represents the C1s spectrum of the galled surface at 300 °C. The percentage of sp^3 hybridized carbon decreased from 64% (as deposited) to 16% at 300 °C. The decrease in the concentration of sp^3 hybridized carbon directly affects the strength of the coating.

Concurrently, the concentration of sp^2 hybridized carbon increased as the concentration of sp^3 hybridized carbon decreased at 300 °C. The C1s spectrum of the galled surface also showed satellite peaks around 289.0, 292.0, and 295.0 eV corresponding to C=O, π -π*(1), and π -π*(2) bonds, respectively [291]. The π bond is a characteristic of sp^2 hybridized carbon, where the 2s orbital of carbon atom mixes with only two of the three available 2p orbitals. The remaining one singly occupied 2p orbital mixes with another singly occupied 2p orbital to form a π -π* conjugate bond. The rise in the percentage of sp^2 hybridized carbon would have resulted in the formation of π -π* conjugate bonds. The Mo3d orbital spectrum of galled samples is shown at RT and 300 °C (**Figure** 5.17(b)). At RT, the $Mo3d_{5/2}$ and $Mo3d_{3/2}$ orbital peaks were found to be around 228.0 and 231.0 eV, respectively, indicating the presence of Mo from the coating. After the galling test at 300 °C, the $Mo3d_{5/2}$ and $Mo3d_{3/2}$ orbital peaks shifted to 232.8 and 235.7 eV, respectively. The peaks at these binding energy correspond to the Mo^{6+} oxidation state in MoO_3 [292].

Although, the decrease in the concentration of sp^3 hybridized carbon at high temperatures reduced the strength of the coating. The coating was still able to outperform steel because of the formation of lubricious MoO_3 at high temperatures. Therefore, at high temperatures, no signs of tribochemical reactions were observed. The galling characteristics of the coating depend on the chemical changes occurring in the composition of the coatings at a higher temperature, i.e., an increase in the percentage of sp^2 hybridized carbon and the formation of MoO_3.

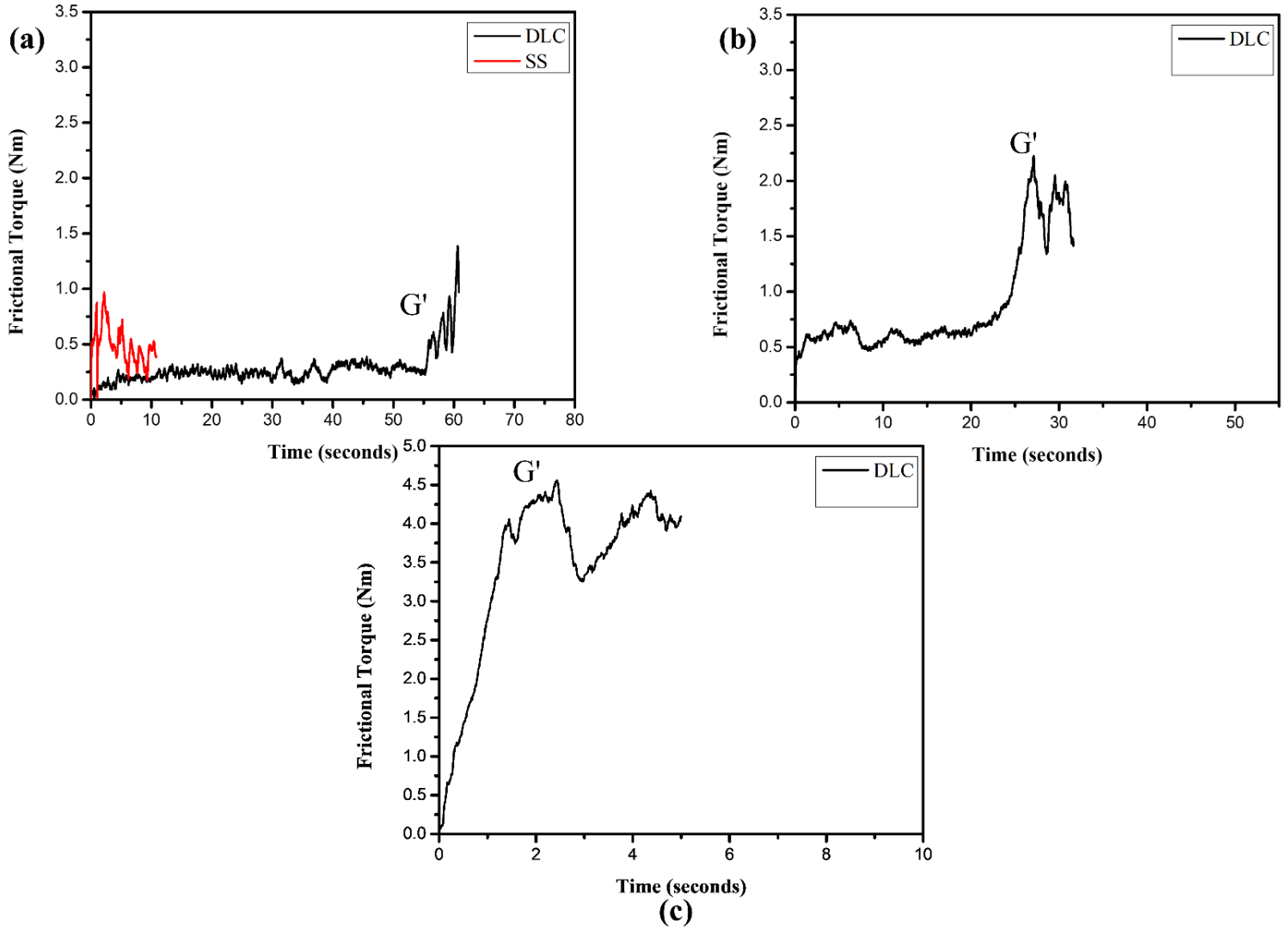

Figure 5.16. Friction torque curves of the tribopairs obtained at 300 °C (a) 2 MPa (b) 5 MPa and (c) 7 MPa.

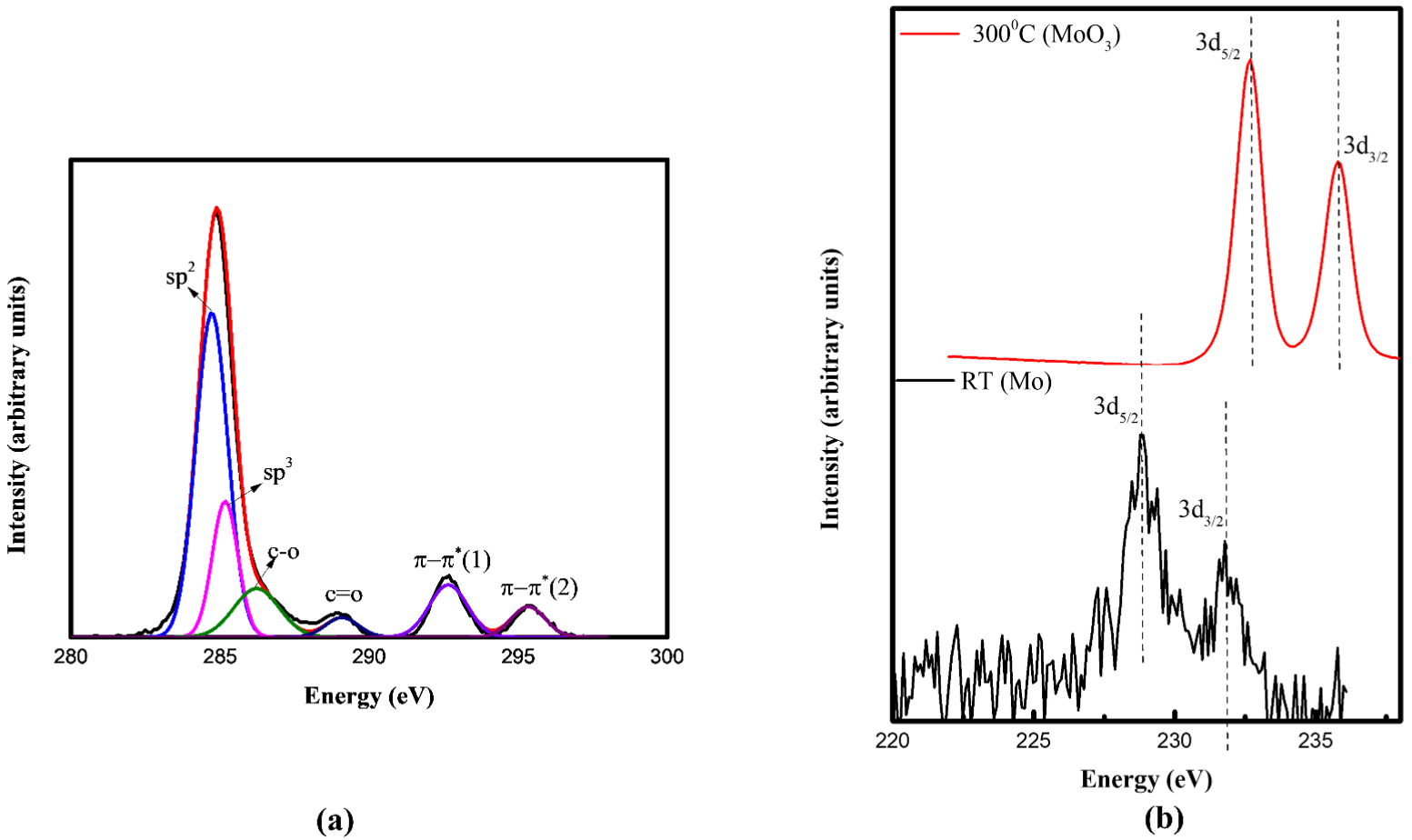

Figure 5.17. (a) C1s spectrum of the galled sample at 300 °C and (b) Mo3d spectrum of the galled sample at RT and 300 °C.

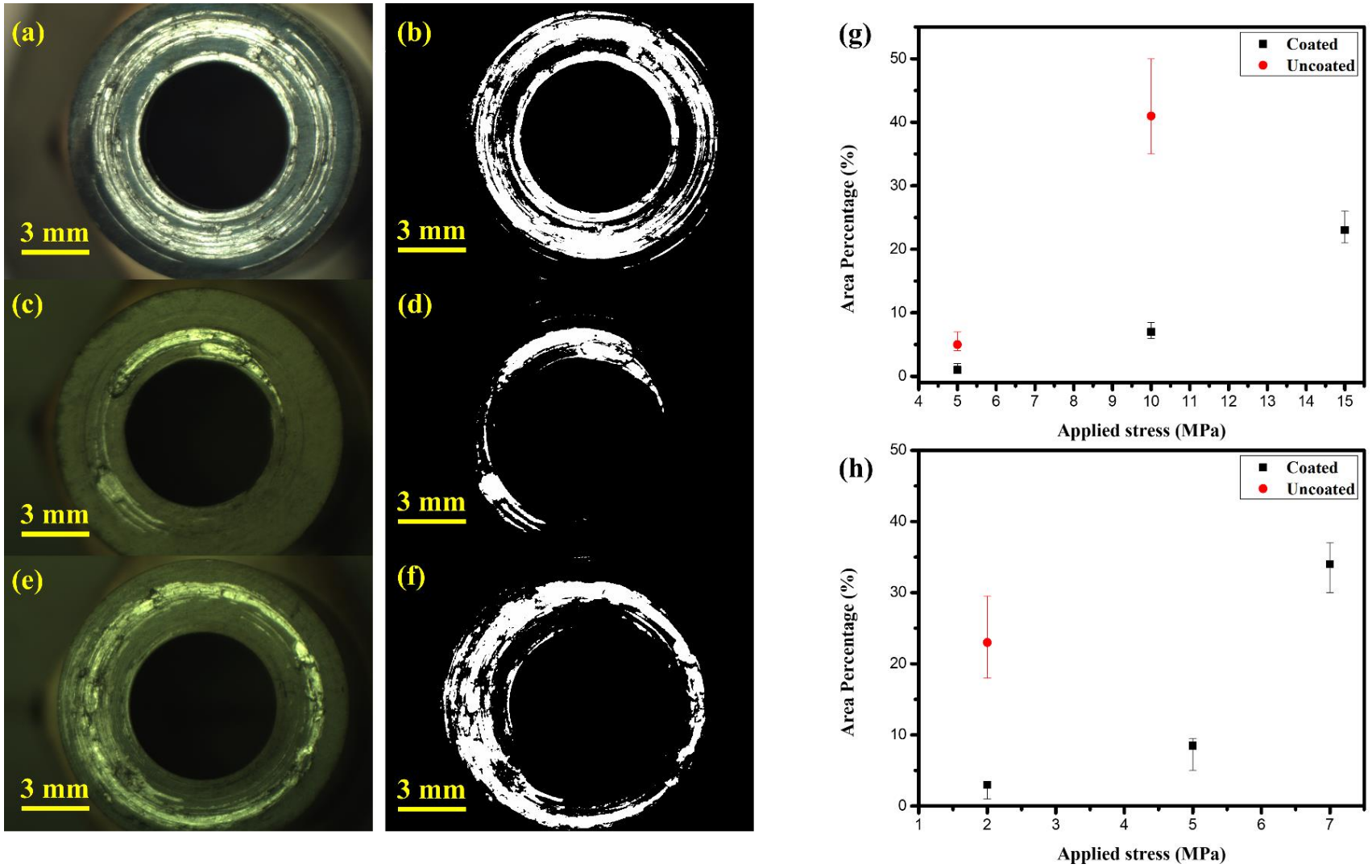

Figure 5.18. (a-h) Stereo-zoom images of galled surface along with their respective processed images (g) plot of galled area across different applied stresses at RT and (h) 300 °C.

5.3.2.6. Comparison of coated and uncoated galled surface.

The steel on Mo/DLC multilayer coating tribopair performed better than steel on steel tribopair at RT and 300 °C. **Figure** 5.14 shows that even after failing at greater rotations, the steel on Mo/DLC multilayer coating tribopair showed a lower galled area than steel on steel tribopair. These areas were extracted and calculated for all the galled surfaces through image processing and computer vision tools. The stereo-microscopic images of galled samples and their processed image for calculation of area have been shown in **Figure** 5.18 (a-f).

Figure 5.18 (g) shows the average galling area of the samples tested at RT. The worn area of steel on Mo/DLC multilayer coating tribopair was lower than steel on steel tribopair. The uncoated tribopair also showed significant variations in the worn area at higher load at different tests. The coated tribopair did not show any significant variations in the worn area, even at higher loads. The same kind of relationship was also seen for samples tested at 300 °C. However, the uncoated samples exhibited a considerable amount of wear at 2 MPa at 300 °C. Therefore, tests at higher load were only conducted for coated samples.

FESEM images were taken for the radial cross-section of the coated and uncoated samples tested at 10 MPa. From **Figure** 5.19, a new layer is formed just below the galled surface. This layer has been termed as a tribologically transformed zone or tribologically activated zone [2,283]. Very little has been reported on tribologically transformed zone in the literature. Samuel et al. also observed this zone during the galling test of SS 316L. The material undergoes severe microstructural changes in the tribologically activated zone, and the region is nanocrystalline and has high hardness [283]. Besides a tribologically activated zone, the coated sample (**Figure** 5.19 (a)) had a wear scar and some leftover coating material. In contrast, the uncoated sample showed severe wear and signs of ploughing on the surface. The height of the tribologically transformed zone was also found to be different for both samples. The height of the tribologically transformed zone was 84.6 and 31.6 μm for coated and

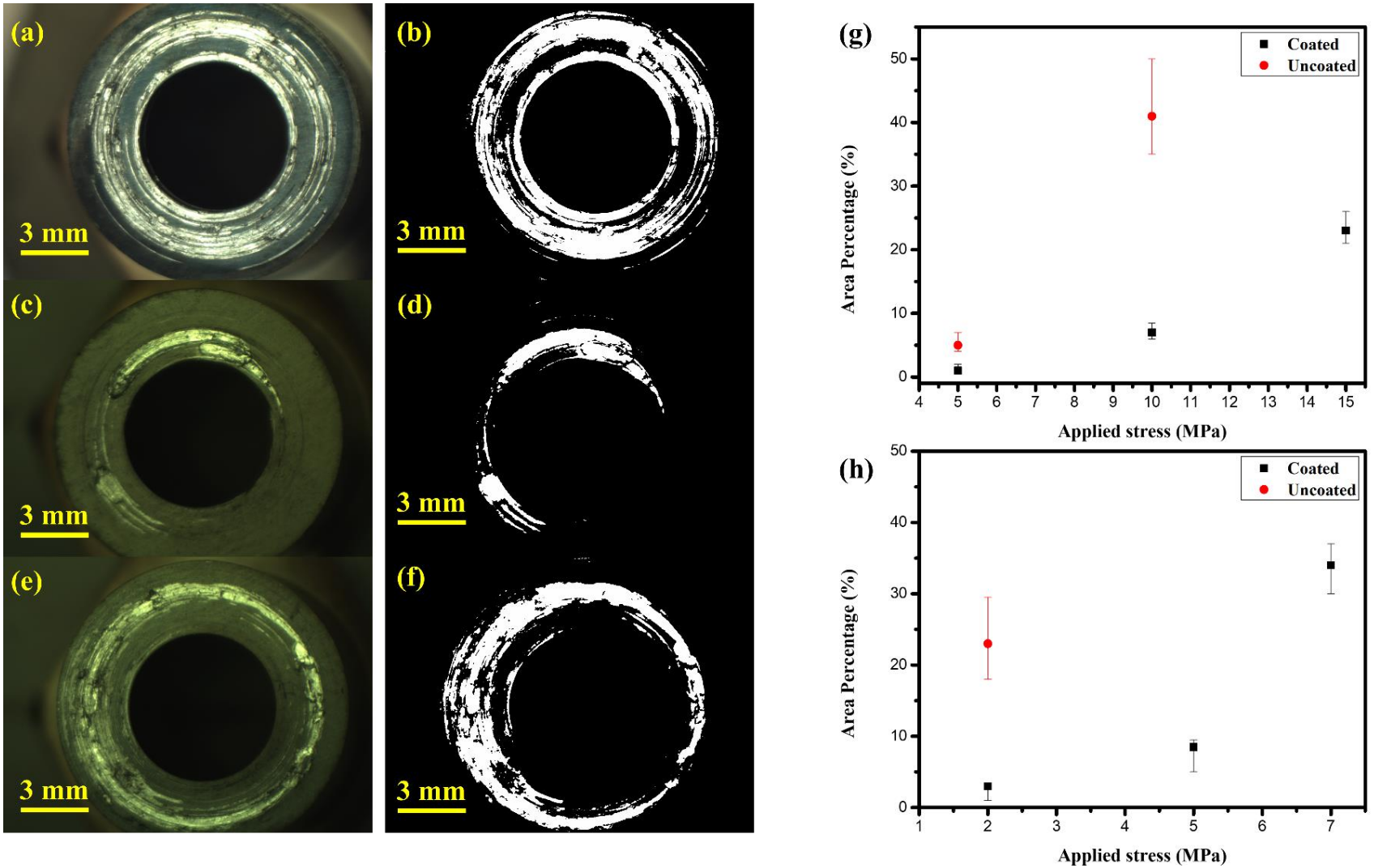

Figure 5.19. (a-h) Stereo-zoom images of galled surface along with their respective processed images (g) plot of galled area across different applied stresses at RT and (h) 300 °C.

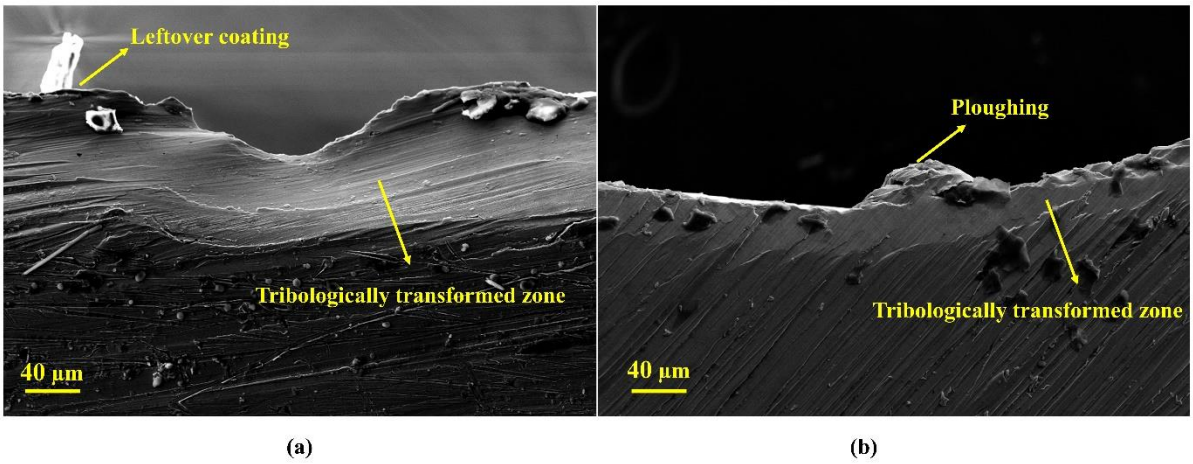

Figure 5.20. Radial cross-section SEM images of galled surfaces (a) coated and (b) uncoated.

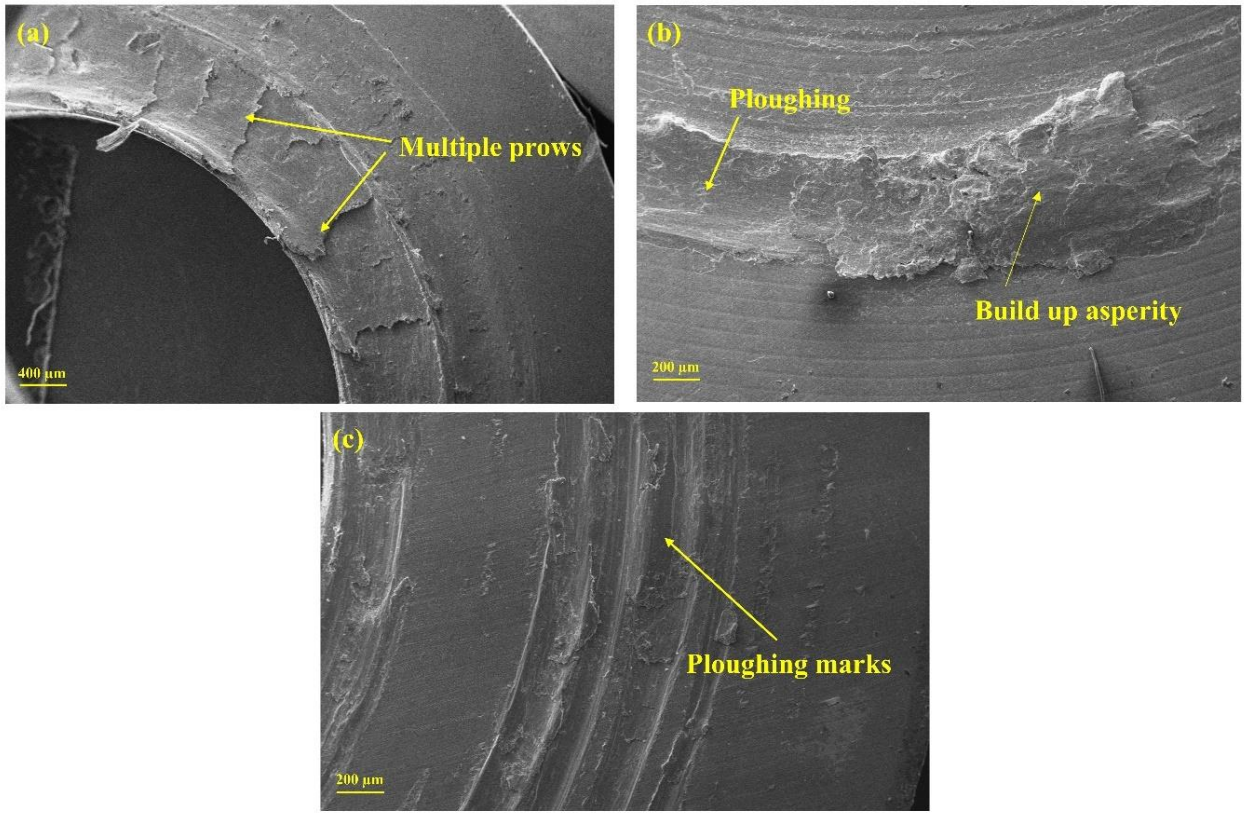

Figure 5.21. SEM images of the top surface of the galled surface (a) steel (steel on steel tribopair) (b) uncoated sample (steel on Mo/DLC multilayer coating tribopair) and (c) coated sample (steel on Mo/DLC multilayer coating tribopair).

uncoated samples, respectively. This height difference would have been due to the difference in the testing time of the two samples. The coated samples have galled at more rotations than the uncoated one, leading to more microstructural changes below the worn surface.

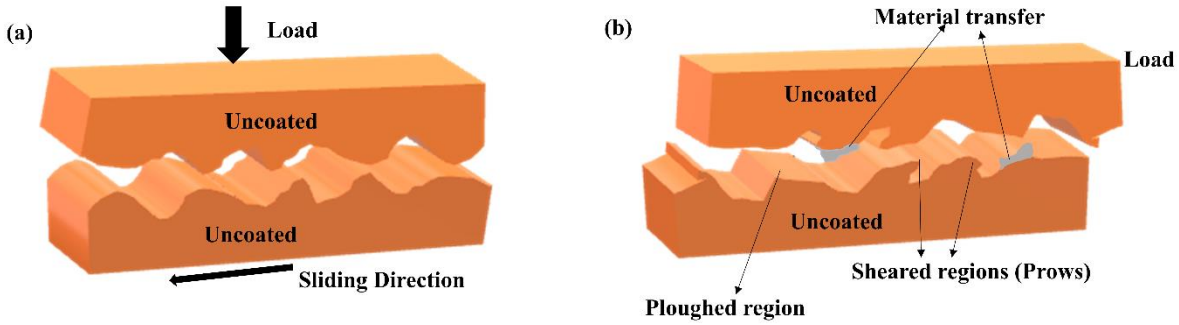

Figure 5.22. Schematic representation of the mechanism of galling in steel on steel tribopair; (a) asperities come into contact having strong adhesive forces and (b) material transfer and prows being formed.

FESEM images of the top surfaces of both tribopairs were analyzed (**Figure** 5.20). **Figure** 20 (a) shows the FESEM image of the galled surface of steel on steel tribopair at 10 MPa. Whereas, **Figures** 5.20 (b) and (c) shows the galled surface of steel and coated sample, respectively on steel on Mo/DLC multilayer coating tribopair at 10 MPa. The galled surface of the steel sample from steel on steel tribopair (**Figure** 5.20 (a)) showed multiple prows on the surface. In steel on steel tribopair, when the surfaces come in contact, adhesion takes place. The asperities in contact form an adhesive junction. When sheared, these adhesive junctions form wedge-like formations and result in formation of prows (**Figure** 5.21) [283]. The mechanism of galling in steel on Mo/DLC multilayer coating tribopair was slightly different from steel on steel tribopair. The steel and coated samples of steel on Mo/DLC multilayer coating tribopair showed the presence of ploughing marks and a build-up asperity at the end of the ploughing (**Figure** 5.20 (b) and (c)). When the coated and uncoated samples come in contact, the hard and smooth coating surface shears the asperities on the uncoated surface. The asperities ploughed through the surface of uncoated specimen, forming a build-up asperity at

the end (**Figure** 5.22 (b)). The build-up asperity formed due to plastic deformation of the uncoated sample is strain hardened and acts as a stress concentration site for the coated specimen. This strain hardened build up asperity now breaks through the coating due to high contact stresses at its tip and ploughs through the coated surface (**Figure** 5.22 (c)). Since all the tests were conducted until the failure, a similar amount of damage area was observed on both the samples.

5.4.Summary.

- The coating showed good hardness despite the presence of thick Mo layers in between DLC layers because of the dense deposition of DLC layers through the HiPIMS power source.
- The Mo/DLC multilayer coating deposited at the argon flow rate of 15 sccm had the highest sp^3 hybridized carbon concentration and had the best anti-friction and antiwear properties. Also, the coating showed good adhesion to the substrate.
- The galling area quantified through computer vision showed that the steel on Mo/DLC multilayer coating tribopair observed less galling damage than steel on steel tribopair in all test conditions. Also, the fluctuations in galled area across various tests were more in steel on steel tribopair than steel on Mo/DLC multilayer coating tribopair.
- At RT, the galling performance of steel on Mo/DLC multilayer coating tribopair was improved, and it was due to the transfer film from coating to the counter-surface. The steel on Mo/DLC multilayer coating tribopair failed at 15 MPa, and in contrast, steel on steel tribopair failed at 5 MPa.
- At 300 °C, the sp^3 hybridized concentration decreased in the coating, but the coated samples still performed better than the uncoated samples because of the formation of lubricious MoO_3. Hence, the steel on Mo/DLC multilayer coating tribopair

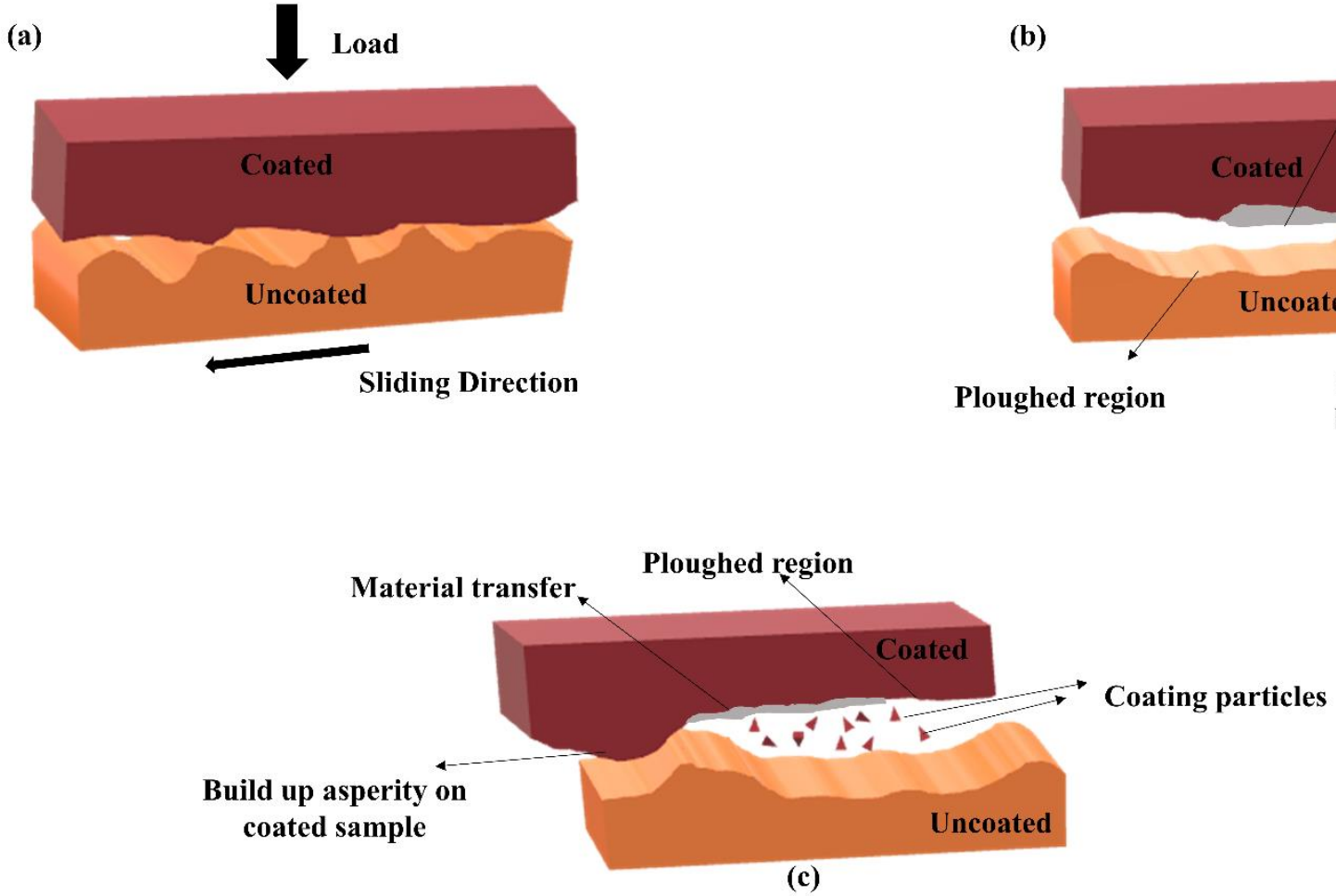

Figure 5.23. Schematic representation of galling mechanism in steel on Mo/DLC multilayer coating tribopair (a) asperities of coated sample and uncoated sample coming into contact, (b) formation of build-up asperity on the uncoated surface, and (c) the strain hardened build up asperity on uncoated surface ploughing the coated surface.

- outperformed than steel on steel tribopair and failed at the load of 7 MPa. The steel on steel tribopair suffered severe damage at 2 MPa only.
- The galled surface of steel on steel tribopair observed a significant amount of plastic deformation and shear failure due to adhesive wear and shearing of asperities.
- The galled surface of steel on Mo/DLC multilayer coating consisted of ploughing marks due to strain hardened asperity build up at the end of ploughed surface on the uncoated surface, which acted as stress concentration sites and exerted huge stresses on the coated surface leading to coating failure.
- A high shear region was observed underneath the galled surface, known as a tribologically transformed zone.